# Development and validation of a TRNSYS Type to simulate the energy performance of solid-gas adsorption thermal storage tanks

Ali Shahrouzian[1], Jean Duquette[1], Ronald Miller[1]
[1]Carleton University, Ottawa, Canada

## Abstract

Adsorption-based thermal energy storage (ATES) is a promising technology for building applications, characterized by its high energy density and minimal heat losses. Nevertheless, its adoption in built environments for heating purposes remains limited, partially due to the lack of comprehensive research pertaining to long-term operation and transient performance modelling of ATES systems. This gap is exacerbated by the absence of specialized components within transient simulation tools like TRNSYS to accurately model and simulate solid-gas ATES tanks. Addressing this challenge is crucial for obtaining reliable approximations of expected results and enabling optimal system design. This paper describes the development of a transient solid-gas ATES tank Type in TRNSYS and its experimental validation using a zeolite 13X – water vapour system. The proposed Type will enable TRNSYS users to assess the performance of solid-gas ATES tanks within larger building-based energy system models.

## Introduction

The International Energy Agency highlights the building sector as the largest global energy consumer, responsible for approximately 40% of the world's total primary energy consumption, and 24% of its $CO_2$ emissions. Notably, heating plays a substantial role in this scenario. (Clark et al., 2020). A key remedy toward low-$CO_2$ buildings involves transitioning from heavy reliance on fossil fuel consumption to renewable energy sources. Solar energy is a promising sustainable energy source that has the potential to replace fossil fuels for a number of heating applications (Cabeza and Chàfer, 2020). However, heat storage technologies are essential for addressing the temporal misalignment between heat supply and demand, and for achieving high solar thermal fractions. (Yan, 2015). Sensible, latent, and sorption/thermochemical energy storage (STCE) are the three categories into which thermal energy storage (TES) can be classified. STCE demonstrates superiority over sensible or latent heat storage methods due to its minimal heat loss during the storage process and higher energy density, resulting in more compact systems. (Solé et al., 2015). Among the different classes of STCES, adsorption thermal energy storage (ATES) technology is considered to be a very attractive solution for further development, especially for non-concentrating solar thermal technologies which are typically employed in the building sector (Xu et al.,2014). The basis of storing and retrieving heat through adsorption technology involves a reversible reaction between the sorbent and sorbate, and consists of three phases: charging, storing and discharging. During the endothermic charging process, adsorption materials (working pairs) are heated to undergo dissociation into adsorbent and adsorbate compounds, thereby storing heat. The separated compounds can then be stored individually, typically with negligible energy losses. During the exothermic discharging process, dissociated materials are recombined to retrieve the stored heat (Alebeek et al., 2018). Water, due to its abundance, low cost, and non-hazardous nature, is the preferred adsorbate in ATES systems (Zhang et al., 2017), whereas zeolite and silica gel serve as the most common adsorbent materials (Jarimi et al., 2019).

## Literature Review

A number of studies have been conducted in recent years, both experimentally and numerically, to explore the practical feasibility of integrating long-term ATES systems into building heating applications. Experimental studies have predominantly concentrated on developing and testing laboratory or pilot-scale prototypes of adsorption storage systems, with limited attention given to household-scale implementations. For example, Gaeini et al. (2018) experimentally explored the feasibility of employing a zeolite 13X/water working pair within an ATES system to satisfy domestic hot water (DHW) demands in a household located in the Netherlands. Their study implemented a segmentation reactor concept, comprising four 62.5 L segments operable in both series and parallel modes. Through large-scale pilot experiments, they assessed the energy storage density and power flow dynamics. Charging and discharging processes utilized inlet temperatures of approximately 190°C and 10°C, respectively, with air flow rates of 50 g/s for discharging and 30 g/s for charging the reactor. Optimal operation parameters included a 5-hour charge duration and a 10-hour discharge duration, resulting in a maximum energy density of 198 kWh/m$^3$ at the material level. Running the segments in parallel mode yielded a total

maximum power output of 3.6 kW sustained for nearly 10 hours.

Conducting experiments to assess the performance of such systems can prove to be a challenging, time-consuming, and costly endeavour. A promising alternative involves using numerical modelling and equation solver-based simulation tools (such as TRNSYS) as these may reduce the need for constructing expensive test rigs (Cheng et al., 2017). However, numerical modelling studies of ATES systems are few and far between relative to their experimental counterparts. Notably, the majority of numerical investigations in this domain have concentrated on constructing mathematical models to simulate the transport phenomena within a heat storage reactor.

Tatsidjodoung et al. (2016) investigated a zeolite-based ATES system to meet the space heating demands of a modern family house. They developed an experimental system consisting of two 70-liter cylindrical tanks capable of delivering approximately 2 kW of heat during the discharging process. Inlet air temperatures to the storage tanks were maintained at 120°C and 180°C during the charging phase, and 120°C during the discharging phase. Air was blown into the storage tanks at constant flow rates of 120 and 180 $m^3$/h during both processes. The study also introduced a dynamic 1D model to forecast the charging and discharging processes within the adsorption tanks. Governing equations describing the system's behaviour were discretized using the finite volume method (FVM), and the discretized equations were solved using the DASSL integration algorithm of the Dymola solver. The simulation results were then compared to the experimental results. Some discrepancies between the experimental and simulation results were observed during both the charging and discharging tests. Gaeini et al. (2016) conducted experimental and numerical investigations to assess the thermal dynamics of an ATES system. Their lab-scale setup featured an adsorption tank with a volume of 0.42 liters, utilizing water-zeolite 13X as the working pair. During the discharging process, they employed a fixed inlet temperature of approximately 15.5°C with an air flow rate of 3.6 $m^3$/h. The numerical model was implemented in COMSOL Multiphysics, a Finite Element Method (FEM) based program, utilizing the Backward Differentiation Formula (BDF) scheme with an initial time step of 0.001 s. The duration of simulations was limited to encompassing solely the completion of either the charging or discharging process. Comparisons between numerically calculated and experimentally measured results showed good agreement. In a subsequent study conducted by Gaeini et al. (2017), they developed a 2D mathematical model to evaluate transport phenomenon within the same cylindrical adsorption reactor utilized in their prior study, while accounting for radial effects. Replicating the operational conditions and numerical solution approach from their previous work, they explored their numerical solution. Furthermore, they validated the mathematical model using data obtained from the same experimental setup. Subsequently, they utilized the validated model to investigate the effects of various parameters on the performance of an up-scaled reactor, featuring a volume of 62.5 liters and a larger air flow rate of 144 $m^3$/h. Kuznik et al. (2019) conducted a numerical investigation into the performance of the zeolite reactor tank previously introduced by Tatsidjodoung et al. (2016). They validated their numerical model by utilizing diverse data collected from the previous group's experimental setup, operating under identical conditions. The same solution approach was applied to solve the differential equations governing the system. Smejkal et al. (2020) introduced a novel two-temperature mathematical model for evaluating the thermal performance of a zeolite-based ATES system. Their approach involved developing a numerical solver based on the mixed-hybrid finite element method (MHFEM) and operator splitting technique. They adopted fixed boundary and initial conditions consistent with those employed by Gaeini et al. (2016) for their simulations. The authors stated that utilizing the operator splitting technique led to significantly more efficient computations (with a time step of 0.1 s) compared to treating all numerical solution processes with the same time-stepping scheme. However, they did not validate their numerical findings against experimental data available in the literature. Ferreira et al. (2021) conducted a sensitivity analysis on the operational conditions and design parameters of an ATES system designed for residential heating applications, employing water-zeolite 13X as the reactive pair. They developed a 1D model to describe the conservation equations of mass and heat within the system. Validation of their model was performed using experimental results from the study conducted by Tatsidjodoung et al. (2016). However, no information regarding the numerical solution was provided. Wijayanta et al. (2023) conducted both experimental and numerical investigations to evaluate the thermal performance of an adsorption-based steam generation system with the aim to enhance its efficiency. The experimental setup consisted of a lab-scale adsorption column with a volume of 0.25 liters, filled two-thirds with zeolite 13X particles, and exposed to a stream of moist air with a maximum flow rate of around 0.55 $m^3$/h. Regarding their numerical analysis, they employed the one-dimensional finite difference method (FDM) with a time step of 0.001 seconds to solve the governing equations of the system.

Despite the numerical research efforts outlined above, the integration of adsorption systems into the building sector for heating purposes remains limited. There are several reasons behind this. Firstly, the performance evaluation of such systems is typically done individually, rather than as part of a comprehensive system coupled with building sector components and associated loads. Consequently, outcomes obtained from simulation-based analyses are confined to scenarios where: (a) boundary conditions (temperature,

adsorbate concentration, and velocity) remain fixed throughout simulations over time, neglecting the effects of time-varying conditions imparted from external environmental conditions and other components of the ATES system. However, such circumstances are typically uncommon in real-world conditions unless significant control measures are implemented. (b) adsorption processes are carried out under controlled initial conditions. In a comprehensive system, the initial conditions imposed on the adsorbed phase at the start of the process may vary depending on the performance of other components, the control strategy adopted, and time-dependent ambient conditions. Under various initial conditions, the adsorption bed may function within distinct mass transfer regimes during its operational modes (charging and discharging).

Secondly, despite the existence of a limited number of numerical studies that have examined the performance of adsorber reactors with dimensions and inlet flow rates suitable for building heating applications, the predominant focus in most cases has been on evaluating the mathematical model of the adsorber columns with smaller dimensions and lower inlet flow rates.

Finally, study results are predominantly constrained to simulating ATES systems for short-term operation. Simulating the long-term dynamics of adsorption processes is crucial for providing a comprehensive understanding of system behaviour, ensuring stability, optimizing performance, and addressing practical considerations relevant to real-world applications.

The main objective of this study is to address the existing research gaps outlined above through the development of a new TRNSYS model Type that can be used to simulate the behaviour of a solid-gas ATES tank. The proposed TRNSYS Type will help users in evaluating the performance of solid-gas ATES tanks across several key aspects: (1) integration within larger building-based energy system models, (2) time-variant operational conditions, (3) and long-term operations. Moreover, the proposed Type will facilitate the designing and sizing of other peripheral parts of a completed ATES system for meeting a building's heating requirements under different possible system configurations in an optimal manner. Furthermore, the proposed Type will aid in the development of algorithms that can be used to optimally control the system at any given operating point and help with identifying opportunities for lowering system costs.

## Mathematical model

A mathematical model is developed of a non-adiabatic, and non-isothermal single-component vessel that can capture the dynamic behaviour of a gas-solid ATES system. The ATES system comprises a metallic vessel partially filled with adsorbent solid particles that is insulated on both sides. Teflon serves as a thermal insulator on the inner side of the vessel. During the charging process, a hot inert gas with a negligible content of gaseous adsorbate is introduced into the tank from the top, enabling adsorption within the solid adsorbent particles. Conversely, during the discharging process, a cold inert gas with a considerable content of gaseous adsorbate is introduced into the tank from the bottom, enabling desorption within the solid adsorbent particles. This reversible process is illustrated in Figure 1. For each operational mode, the adsorbent particles remain stationary within the bed, forming a porous medium with an immobile solid structure.

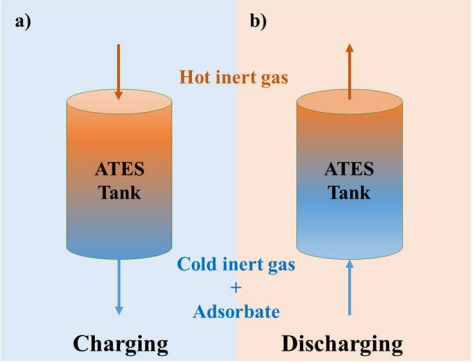


*Figure 1: Operational modes of the adsorption thermal energy storage tank: (a) charging, and (b) discharging.*

The mathematical model describing the proposed ATES system comprises a system of coupled partial differential equations (PDEs), encompassing conservation equations, and an adsorption rate expression, which delineate the dynamic behaviour of dependent variables. The dependent variables are listed in Table 1. In the subsequent subsections, the assumptions, governing PDEs, boundary and initial conditions, and the numerical solution strategy are discussed.

*Table 1: Dependent variables in the mathematical model. $t$ and $x$ are the temporal and spatial coordinates.*

| Dependent variable | Symbol | unit |
|---|---|---|
| Gas phase temperature | $T = T(x,t)$ | K |
| Adsorbate concentration in the gas phase | $c_{ads} = c_{ads}(x,t)$ | mol/m$^3$ |
| Wall temperature | $T_w = T_w(x,t)$ | K |
| Loading of adsorbed species in the solid phase | $q = q(t)$ | mol/kg |

### Assumptions

The equations governing the system dynamics in the model are derived based on the following assumptions:

- A one-dimensional (1-D) modelling approach is adopted to streamline the analysis. Generally, in physical adsorption processes, the 1-D modelling approach has been proven to exhibit satisfactory compatibility with experimental data (Gutiérrez Ortiz, et al., 2019).
- The gas phase is assumed to exhibit ideal gas behaviour.
- The gas and solid phases are in thermal equilibrium.

- The flow pattern in the system is characterized by the axially dispersed plug flow model.
- A Linear Driving Force (LDF) model is used to represent the mass transfer rate between gas and solid.
- The solid adsorbent particles are spherical, possessing identical dimensions and uniform temperature distribution throughout.
- The physical properties of the adsorbent and the tank wall are constant. The velocity variations along the adsorption bed is negligible.
- Radial heat transfer through both the bed and the walls can be represented using a 1-D thermal resistance model.

**Governing equations**

The equations describing the mass, momentum, and energy balances in the adsorption tank are formulated considering the principles of flow mechanics in porous media and the assumptions mentioned above.

The component (adsorbate) mass balance for the gas phase is expressed as

$$\frac{\partial c_{ads}}{\partial t} + u\frac{\partial c_{ads}}{\partial x} = D_x\frac{\partial^2 c_{ads}}{\partial x^2} - \frac{1-\varepsilon_b}{\varepsilon_b}\rho_p\frac{\partial q}{\partial t} \quad (1)$$

where $u$ is the interstitial (physical) flow velocity (m/s), $D_x$ is the axial dispersion coefficient (m$^2$/s) given by the Wakao-Funazkri correlation (Gutiérrez Ortiz, et al., 2019), $\varepsilon_b$ is the bed voidage, and $\rho_p$ is the particle density (kg/m$^3$). The symbols $t$ and $x$ denote time (s) and the axial spatial direction (m), respectively. Equation 1 features two terms on the left-hand side representing the transient and convective aspects, respectively, while the first term on the right-hand side denotes the diffusive aspect. The last term serves as the source/sink term, which represents the mass transfer between the gas and solid phases.

Heat transfer within the adsorption bed, under the assumption of the thermal equilibrium model, is expressed by the following energy conservation equation:

$$(\rho C_P)_{tot}\frac{\partial T}{\partial t} + \varepsilon_b\rho_g C_{P,g}u\frac{\partial T}{\partial x} = k_x\frac{\partial^2 T}{\partial x^2} + (1-\varepsilon_b)\rho_p\frac{\partial q}{\partial t}\Delta H - \frac{2\pi r_{in}}{A_{in}}U_{in}(T-T_w) \quad (2)$$

where $\rho_g$ (kg/m$^3$) is the gas density (kg/m$^3$), $C_{P,g}$ is the gas heat capacity (J/m$^3$K), and $k_x$ is the effective axial thermal conductivity of the gas phase (W/mK) which can be estimated by the Krupiczka correlation (Gutiérrez Ortiz, et al., 2019). $\Delta H$ is the isosteric heat of adsorption (J/mol), $r_{in}$ is the inner radius (m) of wall assembly (Figure 2), $A_{in}$ is the internal cross-sectional area of the bed (m$^2$), and $U_{in}$ stands for the overall heat transfer coefficient on the inner side of the wall (W/m$^2$.K). Its value is calculated as

$$U_{in} = \frac{1}{2\pi r_{in}R'_{in}} \quad (3)$$

where $R'_{in}$ represents the total thermal resistance per unit length of the column on the inner side (K/mW). This parameter is defined in Figure 2, which also depicts the equivalent thermal circuit of the reactor wall. As shown in Figure 2, $R'_{in}$ includes an effective conduction resistance per unit length term for the Teflon layer and half the stainless steel wall layer, $R'_{cond,in}$ (K/mW), and a heat resistance per unit length term associated with convection between the gas phase and the Teflon layer, $R'_{conv,in}$ (K/mW). The latter term is expressed as

$$R'_{conv,in} = \frac{1}{2\pi r_{in}h_{in}} \quad (4)$$

where $h_{in}$ is the wall heat transfer coefficient (W/m$^2$K) which is obtained from the Li and Finlayson correlation (Gutiérrez Ortiz, et al., 2019).

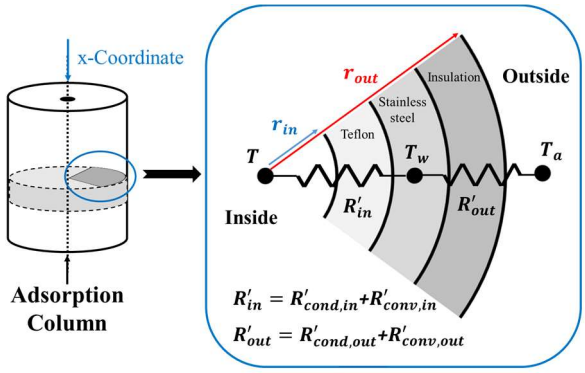


*Figure 2: Equivalent thermal circuit for the reactor wall involving three layers, incorporating four thermal resistances connected in series.*

In Equation 2, the total heat capacity, $(\rho C_P)_{tot}$, (J/m$^3$K) is given by (Gaeini et al., 2016)

$$(\rho C_P)_{tot} = \varepsilon_b\rho_g C_{P,g} + (1-\varepsilon_b)\varepsilon_p\rho_g C_{P,g} + (1-\varepsilon_b)\rho_p C_{P,p} + (1-\varepsilon_b)\rho_p C_{P,p} q C_{P,ads} M_{ads} \quad (5)$$

where $\varepsilon_p$ is the particle porosity, $C_{P,p}$ and $C_{P,ads}$ are the heat capacities of the particles and adsorbate (J/m$^3$K), respectively, and $M_{ads}$ denotes the adsorbate molecular mass (kg/mol). The initial three terms in Equation 2 depict the transient, convective, and diffusive aspects, respectively. The fourth term serves as the source/sink term, indicating the heat transfer between the gas and solid phases. The final term in Equation 2 is a source/sink term that accounts for the heat dissipation from the interior of the reactor bed to its walls due to the temperature gradient between the bed and the wall.

The temperature of the wall can be determined using the following energy balance equation specific to the wall:

$$\rho_w C_{P,w}\frac{\partial T_w}{\partial t} = k_w\frac{\partial^2 T_w}{\partial x^2} + \frac{2\pi r_{in}}{A_w}U_{in}(T-T_w) - \frac{2\pi r_{out}}{A_w}U_{out}(T_w-T_a) \quad (6)$$

where $\rho_w$, $C_{P,w}$ and $k_w$ represent the density (kg/m$^3$), heat capacity (J/m$^3$K) and thermal conductivity (W/mK) of the bed wall, respectively. $T_a$ is the ambient temperature (K). $A_w$ represents the cross-sectional area (m$^2$) of the body of the column wall. $r_{out}$ is the outer radius (m) of the wall

assembly (Figure 2), and $U_{out}$ is the overall heat transfer coefficient on the outer side of the wall (W/m$^2$K). Its value is calculated as

$$U_{out} = \frac{1}{2\pi r_{out} R'_{out}} \quad (7)$$

where $R'_{out}$ (defined in Figure 2) represents the total thermal resistance per unit length on the outer side and includes an effective conduction resistance per unit length term for the insulation layer and half the wall layer, $R'_{cond,out}$ (K/mW), and a resistance per unit length term associated with convection between the wall and the ambient air, $R'_{conv,out}$ (K/mW). The latter term is calculated using the Morgan correlation (Incropera et al., 2007), which is applicable for external free convection across long vertical cylinders. In Equation 6, the transient term is situated on the left-hand side, while the first term on the right-hand side denotes the diffusive term. The last two terms function as source/sink terms and represent heat transfer between the wall assembly and its surroundings, including the gas phase and ambient air.

The component mass balance equations and the energy balance equation for the gas phase contain a source/sink term associated with the adsorption kinetics. The linear driving force (LDF) model stands out as the most commonly used among existing kinetic models for monitoring adsorption processes, valued for its simplicity, analytical nature, and physical consistency. The LDF approximation, initially introduced by Glueckauf (Gutiérrez Ortiz, et al., 2019), is formulated as

$$\frac{\partial q}{\partial t} = k_{LDF}(q_{eq} - q) \quad (8)$$

where $k_{LDF}$ is the overall mass transfer coefficient (1/s), and $q_{eq}$ is the equilibrium loading of the adsorbate in solid phase (mol/kg). The $k_{LDF}$ coefficient comprises three resistances in series: the external film, the macropore, and the micropore resistances (Ruthven, 1984). Unlike the first two, which align with established empirical and theoretical laws widely recognized within the scientific community, the micropore diffusion resistance reveals significant variations and lacks a dependable predictive theory (Ferreira et al., 2021). Hence, the micropore resistance is disregarded in the present study. The LDF kinetics coefficient is expressed as

$$\frac{1}{k_{LDF}} = \frac{Hd_p}{6k_{film}} + \frac{Hd_p{}^2}{60D_{eff}} \quad (9)$$

where the first term on the right-hand side represents the external film resistance, and the second term on the right-hand side represents the macropore resistance. $k_{film}$ denotes the mass transfer coefficient (m/s) across the external film surrounding the adsorbent particles and is determined using a correlation provided by Wakao and Funazkri (1978), which is applicable for Reynolds numbers ranging from 3 to 10,000. $H$ is the dimensionless Henry's law adsorption equilibrium constant, which is given by (Ruthven, 1984)

$$H = \frac{1}{\varepsilon_b}\rho_s \frac{\partial q_{eq}}{\partial C_{ads}} \quad (10)$$

$D_{eff}$ represents the effective macropore diffusivity (m$^2$/s). This parameter is a function of the molecular and Knudsen diffusivities ($D_M$ (m$^2$/s) and $D_{Kn}$ (m$^2$/s), respectively) and is estimated as (Ruthven, 1984):

$$\frac{1}{D_{eff}} = \frac{\tau}{\varepsilon_p}\left(\frac{1}{D_M} + \frac{1}{D_{Kn}}\right) \quad (11)$$

where $\tau$ is the tortuosity. The Chapman–Enskog theory is employed to estimate $D_M$, while $D_{Kn}$ is obtained from the kinetic theory (Ruthven, 1984). The Langmuir or Langmuir-Freundlich isotherm models are employed to compute the equilibrium adsorbed amount, expressed as (Gaeini et al., 2017)

$$q_{eq} = q_{max}\frac{(bp_{ads})^{\frac{1}{n}}}{1+(bp_{ads})^{\frac{1}{n}}} \quad (12)$$

where $q_{max}$ (mol/kg) represents the maximum amount of adsorbate that can be adsorbed in the solid phase, and $p_{ads}$ (Pa) is the partial pressure of the adsorbate component in the gas phase. The dimensionless parameters $b$ and $n$ are temperature-dependent and are derived as (Gaeini et al., 2017)

$$b = b_0 \exp\left(\frac{\Delta E}{RT_0}\left(\frac{T_0}{T} - 1\right)\right) \quad (13)$$

$$\frac{1}{n} = \frac{1}{n_0} + \gamma\left(1 - \frac{T_0}{T}\right) \quad (14)$$

where $T_0$ represents the reference temperature (K), and $b_0$ and $n_0$ denote the adsorption affinity constant and exponent constant at this temperature, respectively. $R$ is the global gas constant (J/mol.K), and $\Delta E$ is the activation energy for desorption (J/mol). The relationship between $\Delta H$ and $\Delta E$ is given by (Gaeini et al., 2017)

$$\Delta H = \Delta E - \gamma R T_0 n^2 \left(\frac{q}{q_{max} - q}\right) \quad (15)$$

It is worth noting that constants $b_0$, $n_0$, $q_{max}$, $\Delta E$, and $\gamma$ are empirically determined and remain fixed throughout the analysis.

To finalize the mathematical model, the governing equations are given initial and boundary conditions. At the inlet boundary, the dependent variables are subjected to a Dirichlet boundary condition, while, at the outlet surface, a Neumann boundary condition with zero gradient governs these variables. The initial values of all dependent variables are assumed to be known within the domain of interest.

**Numerical solution strategy**

The FVM is employed to discretize the governing equations. The domain of interest is divided into discrete control volumes (cells) using a uniform grid. All dependent variables are defined and evaluated at nodal points located at the centre of the cells, as illustrated in Figure 3. The conservation equations, characterized by the general form:

$$A\frac{\partial \phi}{\partial t} + F\frac{\partial \phi}{\partial x} = D\frac{\partial^2 \phi}{\partial x^2} + S \quad (16)$$

are integrated both in time and space over the cells and subsequently discretized. The time integration is handled

using the implicit technique because of its robustness and unconditional stability. In Equation 16, $\phi$ denotes the dependent variables $T$, $T_w$, and $c_{ads}$. $A$, $F$ and $D$ are coefficients associated with transient, convective, and diffusive terms, respectively, while $S$ represents the source/sink terms. The transient terms in the integrated form of the equations are discretized using the first-order backward difference (BW) method. The central difference (CD) method, which has second-order accuracy, is applied to treat the diffusive terms across the cell faces. A total variation diminishing (TVD) scheme is employed to represent the contribution of the convention terms in the conservation equations.

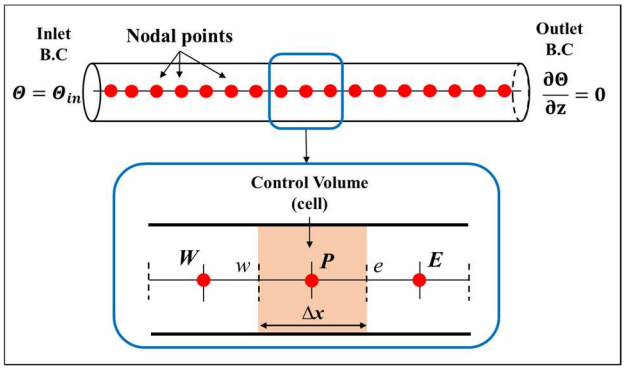


*Figure 3: Uniform grid used for the discretization of governing equations describing the ATES tank model along with the corresponding inlet and outlet boundary conditions. $\Theta$ stands for the dependent variables.*

Using the standard notation introduced in (Versteeg and Malalasekera, 2007), with reference to Figure 3, the discretized form of the mass and energy equations for node $P$ is as follows:

$$A_P \frac{\Delta x}{\Delta t}(\phi_P - \phi_P{}^o) + F_e\left(\phi_P + \frac{1}{2}\psi,(\phi_E - \phi_P)\right) - F_w\left(\phi_W + \frac{1}{2}\psi,(\phi_P - \phi_W)\right) = \frac{D_e}{\Delta x}(\phi_E - \phi_P) - \frac{D_w}{\Delta x}(\phi_P - \phi_W) + S\Delta x \quad (17)$$

where the subscript notation $W$ and $E$ is used to refer to the west and east neighbours of general node $P$, in turn. The notation $w$ and $e$ is used to refer to the west and east cell faces respectively. $\psi$ is a TVD limiter function. Given that the performance of the TVD limiter functions are fairly similar and provide second-order accuracy, the Van Leer limiter function (Versteeg and Malalasekera, 2007) is employed in the present study. $\Delta x$ and $\Delta t$ are spatial and time steps, respectively. In equation 17, the superscript '$o$' refers to variables at time $t$, while variables at time level $t + \Delta t$ are not superscripted. Equation 17 is rearranged to provide the discretised general form of the conservation equations at an internal node $P$ as follows:

$$a_P\phi_P = a_W\phi_W + a_E\phi_E + S_\phi + S_\phi^{DC} \quad (18)$$

where the coefficient $a$ functions as either a TVD central or TVD neighbour coefficient depending on its notation (Versteeg and Malalasekera, 2007). $S_\phi$ is a source/sink term of variable $\phi$, and $S_\phi^{DC}$ denotes a deferred correction source term of the TVD scheme (Versteeg and Malalasekera, 2007). Similar to the conservation equations, the adsorption rate equation (Equation 8) undergoes integration in both time and space followed by discretization. However, unlike the conservation equations, as Equation 8 lacks convection and diffusive terms, the discretized adsorption rate equation at an internal general node $P$ takes the form

$$a'_P q_P = S_q \quad (19)$$

where $a'_P$ and $S_q$ are the central coefficient and source/sink terms of variable $q$, respectively.

The discretization process, eventually, yields four linear algebraic equations for each nodal point, encompassing equations for $T$, $T_w$, $c_{ads}$, and $q$. The resulting tri-diagonal system of linear algebraic equations is then solved using the Gauss-Jordan method in each time step.

## Validation and Results

The proposed ATES model is coded in Fortran90 as this is the programming language utilized by most Types in the TRNSYS standard component library. The model (specifically the discharging process) is validated using experimental data from the literature. The aim of the validation is to demonstrate the accuracy and versatility of the proposed model. Experimental results from the study conducted by Gaeini et al. (2016) are chosen for the validation. This study offers a comprehensive dataset that includes detailed experimental parameters and conditions. Table 2 summarizes the key details of the study such as the properties of the adsorbent (*i.e.,* zeolite 13X), the tank characteristics, and the operational conditions of the adsorption experiment. Further details regarding the experimental setup can be obtained from (Gaeini et al., 2016).

*Table 2: Adsorbent properties (zeolite 13X), tank characteristics, and operational conditions used for validation of proposed ATES model (Gaeini et al., 2016).*

| Property | Value |
|---|---|
| Bed porosity ($\varepsilon_b$) | 0.35 |
| Particle density ($\rho_p$) | 1152 kg/m$^3$ |
| Particle heat capacity ($C_{P,p}$) | 880 J/kg.K |
| Bed height ($L$) | 0.11 m |
| Wall assembly inner radius ($r_{in}$) | 0.07 m |
| Teflon layer thickness ($th_{Teflon}$) | 0.005 m |
| Stainless steel layer thickness ($th_{ss}$) | 0.01 m |
| Insulation thickness ($th_{ins}$) | 0.03 m |
| Wall heat capacity ($\rho_w C_{P,w}$) | 3064 kJ/m$^3$.K |
| Air flow rate ($Q_{in}$) | 1 l/s |
| Inlet water concentration ($c_{ads,in}$) | 0.3 mol/m$^3$ |
| Ambient temperature ($T_a$) | 21.5 °C |

The lab-scale setup of Gaeini et al. (2016) includes a 0.42-liter ATES tank, that employs water-zeolite 13X as the working pair. The initiation of the discharging process in the tank is triggered by introducing cold moist air from the top,

under operational conditions specified in Gaeini et al. (2016). This leads to the adsorption of water vapour in the zeolite and the subsequent release of heat. Figure 4 illustrates a comparison between the simulation results of the proposed model and the experimental data from the work conducted by Gaeini et al. (2016). Specifically, the focus is on the outlet temperature profile ($T_{out}$) of the gas phase during the adsorption process.

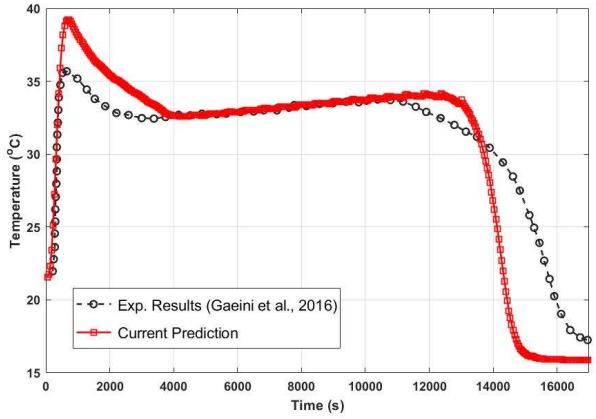


*Figure 4: Variation in the outlet gas temperature during the discharging process for the proposed model (i.e., current prediction) and the reference study by Gaeini et al. (2016).*

The proposed model (*i.e.,* current prediction) is in reasonable agreement with the results from the reference study. However, discrepancies are observed between the numerical results and experimental data at both the beginning and end of the process. This effect is attributed to the assumption of constant gas velocity in the model. In practice, during the discharging process, the gas velocity within the tank increases due to two primary factors: the acceleration of the gas resulting from mass loss (water vapour) and the presence of a pressure drop. This implies that the gas spends less time within the tank compared to the scenario where constant velocity is assumed. Consequently, at the onset of the process, the gas absorbs less released heat, and at the end of the process, it dissipates less heat into the ambient surroundings.

To evaluate the accuracy of the model across various spatial points within the tank and validate the simulation's ability to capture temperature variations throughout the system, comparisons are made between temperatures at different levels of the tank using the propose model and experimental data. Figure 5 illustrates this comparison and demonstrates a good agreement between the current predictions and those from the reference study.

Figure 6 compares the proposed model's predictions with both the experimental and numerical results obtained by Gaeini et al (2016) for the water vapour concentration at the outlet of the tank. This comparison demonstrates that the proposed TRNSYS Type provides a closer match to the experimental data compared to the numerical outcomes of the reference study. As illustrated in Figure 6, the concentration of water vapour at the outlet of the bed remains at zero until the zeolite particles within the bed begin to saturate. Subsequently, the concentration of water vapour gradually increases as more zeolite particles become saturated with water. Eventually, all zeolite particles within the bed become completely saturated with water, causing the concentration of water vapour to reach its initial value at the inlet, indicating that no further adsorption occurs inside the bed.

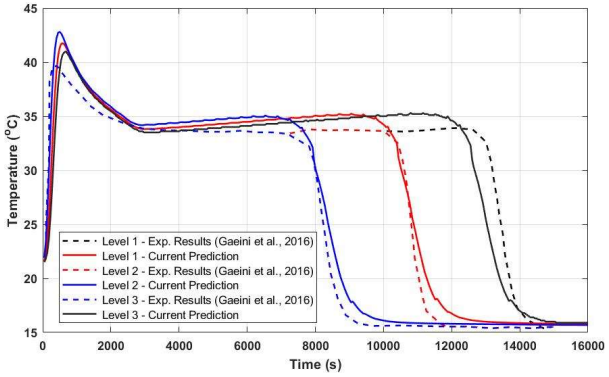


*Figure 5: Variation in the outlet gas temperature at different levels of the tank during the discharging process for the proposed model (i.e., current prediction) and the reference study by Gaeini et al. (2016).*

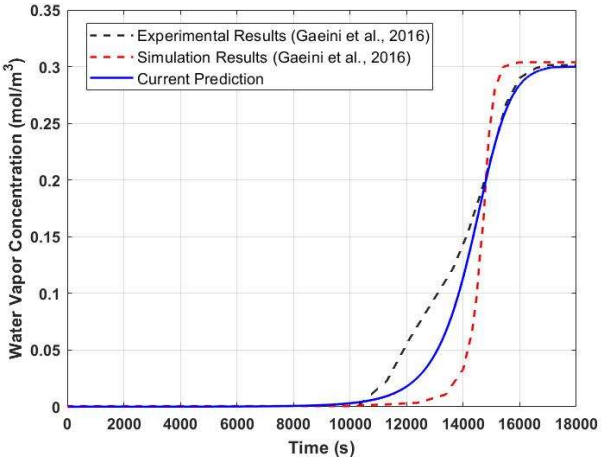


*Figure 6: Variation in the outlet water vapour concentration during the discharging process for the proposed model (i.e., current prediction) and the reference study by Gaeini et al. (2016).*

## Conclusion

In this study, a new TRNSYS Type written in Fortran90 has been developed for conducting transient simulations of a gas-solid ATES tank. The proposed model was validated using experimental data from a reference study in the literature. The comprehensive comparison made between the proposed model and the reference study attests to the validity and robustness of new TRNSYS Type.

An important area of future work will include addressing the minor discrepancies observed between the numerical results and experimental data at the initiation and conclusion of the discharging process. This will be achieved by examining the impacts of velocity variations throughout the adsorption processes on the dependent variables. Additionally, given the model's intended application for long-term simulations, a deeper exploration is warranted into the time step necessities of transient simulations, considering specific mesh sizes and operational conditions.

The work presented in the current study was conducted as part of the initial phase of a long-term project focused on evaluating the performance of solid-gas ATES tanks. The proposed TRNSYS Type will facilitate the design and sizing of ATES-based heating systems. Through its implementation, users will be able to effectively assess, control, and optimize ATES systems, ushering in a new era of efficiency and sustainability in building energy management.

## Acknowledgement

This research is supported by the funding provided by the National Sciences and Engineering Research Council (NSERC) of Canada and from an endowment funded by the Borealis Foundation.

## References

Clark, R.J. Mehrabadi, A., Farid, M. (2020). State of the art on salt hydrate thermochemical energy storage systems for use in building applications. *J. Energy Storage*. 27.

Cabeza, L.F. and Chàfer, M. (2020). Technological options and strategies towards zero energy buildings contributing to climate change mitigation: A systematic review. *Energy Build*. 219, 110009.

Yan, T., Wang, R.Z., Li, T.X., Wang, L.W., Fred, I.T. (2015). A review of promising candidate reactions for chemical heat storage. *Renew. Sustain. Energy*. Rev. 43.

Solé, A., Martorell, I., Cabeza, L.F. (2015). State of the art on gas–solid thermochemical energy storage systems and reactors for building applications. *Renew. Sustain. Energy*. Rev. 47, 386–398.

Xu, J., Wang, R.Z., Li, Y. (2014). A review of available technologies for seasonal thermal energy storage. *Sol. Energy*. 103, 610–638.

Van Alebeek, R., Scapino, L., Beving, M.A.J.M., Gaeini, M., Rindt, C.C.M., Zondaga, H.A. (2018). Investigation of a household-scale open sorption energy storage system based on the zeolite 13X/water reacting pair. *Appl. Therm. Eng*. 139, 325–333. 610–638.

Zhang, Y.N., Wang, R.Z., Li, T.X. (2017). Experimental investigation on an open sorption thermal storage system for space heating. *Energy*. 141, 2421–2433.

Jarimi H., Aydin D., Yanan Z., Ozankaya G., Chen X., Riffat S. (2019). Review on the recent progress of thermochemical materials and processes for solar thermal energy storage and industrial waste heat recovery. *Int J Low-Carbon Technol*. 14, 44–69.

Gaeini, M., Van Alebeek, R., Scapino, L., Zondag, H.A., Rindt, C.C.M. (2018). Hot tap water production by a 4 kW sorption segmented reactor in household scale for seasonal heat storage. *J. Energy Storage*. 17, 118–128.

Cheng, D., Peters, E.A.J.F., Kuipers, J.A.M. (2017). Performance study of heat and mass transfer in an adsorption process by numerical simulation. *Chemical Engineering Science*. 160, 335–345.

Tatsidjodoung, P., Le Pierrès, N., Heintz, J., Lagre, D., Luo, L., Durier, F. (2016). Experimental and numerical investigations of a zeolite 13X/water reactor for solar heat storage in buildings. *Energy Convers. Manag*. 108, 488–500.

Gaeini, M., Zondag, H.A., Rindt, C.C.M. (2016). Effect of kinetics on the thermal performance of a sorption heat storage reactor. *Appl. Therm. Eng*. 102, 520–531.

Gaeini, M., Wind, R., Donkers, P., Zondag, H.A., Rindt, C.C.M. (2017). Development of a validated 2D model for flow, moisture and heat transport in a packed bed reactor using MRI experiment and a lab-scale reactor setup. *Int. J. Heat Mass Transfer*. 113, 1116–1129.

Kuznik, F., Gondre, D., Johannes, K., Obrecht, C., David, D. (2019). Numerical modelling and investigations on a full-scale zeolite 13X open heat storage for buildings. *Renew. Energy*. 132, 761–772.

Smejkal, T., Mikyˇska, J., Fuˇcík, R. (2020). Numerical modelling of adsorption and desorption of water vapor in zeolite 13X using a two-temperature model and mixed-hybrid finite element method numerical solver. *Int. J. Heat Mass Transf*. 148, 119050.

Ferreira S., Sochard S., Serra S., Marias F., Reneaume J-M. (2021). Modelling of an adsorption heat storage system and study of operating and design conditions. *Processes*. 9(11), 1885.

Wijayanta, A.T., Hironaka, S., Hanaki, M., Fukai, J. (2023). Heat generation in a packed bed of zeolite particles using moist air. *Int. J. Refrig*. 152, 269-282.

Guti´errez Ortiz, F.J., Barragan ´ Rodríguez, M., Yang, R.T. (2019). Modeling of fixed-bed columns for gas physical adsorption. *Chem. Eng. J*. 378, 121985.

Incropera, F.P., Dewitt, D.P., Bergman, T.L., Lavine, A.S. (2007). *Fundamentals of Heat and Mass Transfer*. Sixth Ed., John Wiley & Sons, New York.

Mahmoudi, Y., Hooman, K., Vafai, K. (2019). *Convective Heat Transfer in Porous Media*. CRC Press.

Ruthven, D.M. (1984). *Principles of Adsorption and Adsorption Processes*. John Wiley & Sons, New York.

Versteeg, H.K., Malalasekera, W. (2007). *An Introduction to Computational Fluid Dynamics*. Bill Bain Limited, Glasgow.